Chemical Papers (2023) 77:5331–5342
https://doi.org/10.1007/s11696-023-02865-6

ORIGINAL PAPER

Synthesis, characterization and effects on biochemical parameters of model organism *Galleria mellonella* L. (Lepidoptera: Pyralidae) of Cu(II) 4-cyanobenzoate with 4-cyanopyridine complex

Mustafa Sertçelik[1] · Serkan Sugeçti[2] · Füreya Elif Öztürkkan[1] · Tuncer Hökelek[3]

Received: 6 March 2023 / Accepted: 9 May 2023 / Published online: 1 June 2023

Abstract

The structure of the title complex, $C_{56}H_{32}Cu_2N_{12}O_8$, was characterized using elemental analysis, Fourier transform infrared (FT-IR) spectroscopy and single-crystal X-ray diffraction technique. In addition, the effects of the newly synthesized complex on metabolic, antioxidant and biochemical parameters of *Galleria mellonella* larvae were investigated. In the title dinuclear Cu^{II} complex, $[Cu_2(C_6H_4N_2)_4(C_8H_4NO_2)_4]$, the metal atom is chelated by one carboxylate group from 4-cyanobenzoate (CYNB) anion and coordinated by two 4-cyanopyridine (CYNP) anions; two carboxylate O atoms from the two CYNB anions bridge to the Cu atom, completing the six-coordination geometry. The two axial locations of the two 4-cyanopyridine (CYNP) N atoms complete the distorted octahedral coordination, which is formed by the four carboxylate O atoms in the equatorial plane around the Cu^{II} atom. In the crystal, the weak C–H·N hydrogen bonds link the molecules into a network architecture, in which they may be effective in the stabilization of the structure. A weak C–H π interaction also further consolidates the crystal packing. According to the Hirshfeld surface study of the crystal structure, the interactions between H N/N H (31.8%), H H (21.3%), H C/C H (18.2%) and C C (11.1%) are the most significant ones for the crystal packing. The two main types of interactions in crystal packing are hydrogen bonds and van der Waals interactions. In this study, metabolic enzyme activities and amount of non-enzymatic antioxidants were increased in hemolymph of *G. mellonella* larvae exposed to newly synthesized complex. The results of this study showed that newly synthesized complex could be a potential chemical against pests.

Keywords 4-cyanobenzoate · 4-cyanopyridine · XRD · Copper complex · *Galleria mellonella* · Transferase enzymes · Metabolic enzymes · Pest control

Introduction

Materials science and the design of new materials have an important place in the industry. The properties of all newly designed materials vary depending on the variety of structures (Öztürkkan Özbek et al. 2020). Therefore, metal complexes have wide research areas in materials science (Li et al. 2019; El-Shwiniy et al. 2021; Sugeçti and Büyükgüzel 2022; Topal 2022). These metal-centered compounds form metal complexes in coordination with organic or inorganic ligands. These compounds can have a mononuclear, binuclear or polymeric structure (Hökelek et al. 2009a, b, c b, c; Sertçelik et al. 2012b; Sertçelik and Durman 2020). These variations in their structures play a major role on the chemical, physical and biological properties of the synthesized compound (Öztürkkan Özbek et al. 2020). It is known that both aromatic carboxylic acids and N- and O-donor aromatic carboxylic acid derivatives, which are used as ligands in the formation of metal complexes, show biological activity (Sertçelik et al. 2021; Sertçelik 2021). In addition, it is known that metal complexes of aromatic carboxylic acids show antifungal, anti-bacterial, anti-tumor and anticancer activities and also insecticide effects (Zeng et al. 2021;

✉ Mustafa Sertçelik
mustafasertcelik@kafkas.edu.tr;
mustafasertcelik@gmail.com

[1] Department of Chemical Engineering, Faculty of Engineering and Architecture, Kafkas University, 36300 Kars, Turkey

[2] Department of Veterinary Medicine, Çaycuma Food and Agriculture Vocational School, Zonguldak Bülent Ecevit University, 67100 Zonguldak, , Turkey

[3] Department of Physics, Hacettepe University, 06800 Beytepe, Ankara, Turkey

Narayana and Sung-Ok 2017; Uddin et al. 2020; Sertçelik et al. 2018).

Insecticides used in the management of pests cause environmental pollution. For this reason, it has gained importance to investigations for alternative chemicals to insecticides that pose a threat to the environment and humans. As an alternative to insecticides in the management of pests, biological and chemical agents with low toxic effects, such as plant extracts, antibiotics, and metal complexes, have been used recently (Sertçelik et al. 2018; Büyükgüzel and Büyükgüzel 2021; Sugeçti 2021a; Gebremariam et al. 2021).

Galleria mellonella is a pest insect belonging to the order Lepidoptera. In addition, *G. mellonella* is used as an non-mammalian model in many studies such as determining the pathophysiological effects of bacteria, developing new chemicals as alternatives to insecticides, and determining drug toxicity (Kastamonuluoğlu et al. 2020; Altuntaş et al. 2022).

Biochemical parameters and antioxidant systems are affected by exposure to chemicals in organisms. Oxidative stress caused by chemical agents causes an increase in cell damage indicator enzymes such as aspartate aminotransferase (AST), alanine aminotransferase (ALT) and lactate dehydrogenase (LDH) in organisms (Sertçelik et al. 2018; Sugeçti 2021b). In addition, metabolic enzyme activities such as alkaline phosphatase (ALP), creatine kinase (CK) and amylase (AMYL), which regulate energy metabolism, increase as an adaptation to oxidative damage (Sugeçti and Büyükgüzel 2018; Tunçsoy et al. 2021). Enzymatic antioxidants, such as catalase (CAT), superoxide dismutase (SOD), gamma-glutamyl transferase (GGT) and glutathione peroxidase (GPx), and non-enzymatic antioxidants, such as albumin (ALB), bilirubin (BIL), glutathione (GLU) and uric acid (UA), play a key role in the prevention of oxidative damage (Haida and Hakiman 2019; Danouche et al. 2020).

In this study, we used 4-cyanobenzoic acid and 4-cyanopyridine in the creation of the novel copper-centered coordination complex. FT-IR spectroscopy, elemental analysis, and single-crystal X-ray diffraction technique were used to further clarify the structure of the synthesized complex. In addition, the insecticide effects of the newly synthesized complex on *G. mellonella* were also investigated.

Experimental

No purification was done before using the synthesis ingredients and solvents: copper(II) sulfate pentahydrate, $CuSO_4$ $5H_2O$ (Sigma-Aldrich); 4-cynobenzoic acid (Sigma-Aldrich); 4-cynopyridine (Sigma-Aldrich). In the range of 4000–600 cm^{-1}, a PerkinElmer Frontier™ FT-IR spectrometer with solid samples and a Diamond ATR Accessory were used. The elemental analyzer LECO CHNS-932 was used to perform the C, H and N microanalyses.

Synthesis of the complex

In beakers with 50 mL of water, sodium bicarbonate (10 mmol, 0.84 g) and 4-cyanobenzoic acid (10 mmol, 1.89 g) were combined to create sodium 4-cyanobenzoate salt. After that, the mixture was continuously agitated at 60 °C to release all of the CO_2 gas. In a separate beaker, 50 mL of water was used to dissolve $CuSO_4.5H_2O$ (5 mmol, 1.25 g), as well as 4-cyanopyridine (10 mmol, 1.04 g). Sodium 4-cyanobenzoate solution and $CuSO_4.5H_2O$ solution were mixed. At room temperature, the resultant solution was allowed to crystallize. After 6–7 days, the solution was filtered to remove the blue single crystals. The resulting crystals were then washed with a solvent and allowed to dry at room temperature. Anal. Calcd. (%) for Complex, $C_{56}H_{32}Cu_2N_{12}O_8$ (MW = 1128.04) C, 59.63; H, 2.86; N, 14.90. Found (%): C, 59.26; H, 2.27; N, 14.28. Selected IR bands (cm^{-1}): ν(C–N) 2239, $\nu(C–N)_{py.}$ 1052, $\nu COO^-)_{as}$ 1591, $\nu(COO^-)_s$ 1395, $\Delta\nu$ 166, ν(M–O) 651.

X-ray diffraction analysis

On a Bruker APEX-II CCD diffractometer with MoK_α radiation (λ = 0.71073 Å), the crystallographic data of the complex were collected. The SHELX program packages [SHELXT 2014/5 (Sheldrick 2015a), SHELXL2018/3 (Sheldrick 2015b)] were used to handle the absorption corrected data [SADABS V2014/4 (Bruker 2012)] for solving and refining the structures, and the ORTEP-3 for Windows (Farrugia 2012) and PLATON (Spek 2009) programs were utilized for drawings. Geometrically, the locations of the hydrogen atoms were determined at a distance of 0.93 Å (for aromatic CH), and they were then refined using a riding model under the constraints of U_{iso} (H) = 1.2 X U_{eq} (C). During the refinement process, the highest peak ($\Delta\rho_{max}$ = 0.71 e $Å^{-3}$) and the deepest hole ($\Delta\rho_{min}$ = − 0.82 e $Å^{-3}$) were observed 1.14 Å and 0.76 Å away from atoms C16 and Cu1, respectively. The Cambridge Crystallographic Data Centre has received crystallographic information for the structure described here and has stored it there as supporting information under the CCDC No. 2203684. By sending an application to CCDC, 12 Union Road, Cambridge CB2 1EZ, UK, we can request copies of the data. (ccdc.cam.ac.uk; fax: + 44 1223 336,033; email: deposit@ccdc.cam.ac.uk; Web site: http://www.ccdc.cam.ac.uk).

Insect

G. mellonella larvae were collected from the beekeeping area of Zonguldak province and cultured in artificial food under laboratory conditions. Dietary foods are created by mixing wheat bran, strained honey, glycerol, dark honeycomb and water (420gr, 150 ml, 150 ml, 20 gr and 30 ml, respectively) (Bronskill 1961). *G. mellonella* was raised in a Nüve ES 500 incubator with a photoperiod of 12:12 h and environmental conditions of 28.2 °C and 65.5% relative humidity (L:D).

Experimental design and biochemical assay

In this study, 7th instar *G. mellonella* larvae were used in all treatments. Non-lethal concentrations of complex were injected into the abdomen of *G. mellonella* larvae. The hemolymph of *G. mellonella* larvae was collected 24 h after inoculation. Larvae were kept on ice for approximately 5 min for anesthesia, and the surface was sterilized with ethyl alcohol. The hemolymph of *G. mellonella* larvae was collected in Eppendorf tubes using 100 µl Hamilton needle. In this study, 20 larvae were used in each treatment. The experiments were repeated four times. To stop melanization, a few phenylthiourea (PTU) crystals from Sigma-Aldrich in Missouri, USA, were added to the Eppendorf tubes. Samples were kept until analysis at − 80 °C. With the Roche Hitachi Cobas c501 instrument, metabolic enzyme and non-enzymatic antioxidant levels were measured using the appropriate kit (Roche, Germany). Biochemical tests were conducted in accordance with the manufacturers' recommendations.

Table 1 Experimental details

Crystal data	
Chemical formula	$C_{56}H_{32}Cu_2N_{12}O_8$
M_r	1128.04
Temperature (K)	293
Crystal system, Space group	Monoclinic, $P\,2_1/n$
a, b, c (Å)	9.1253 (3), 23.0252 (6), 13.0504 (4)
β (°)	109.788 (2)
μ (mm^{-1})	0.89
V ($Å^3$)	2580.13 (14)
Radiation type	Mo-Kα
Z	2
Crystal size (mm)	0.45 × 0.35 × 0.31
Data (collection)	
Diffractometer	Bruker APEX-II CCD
Absorption correction	Multi-scan
SADABS V2014/4 (Bruker 2012)	
No. of measured, independent as well as observed [$I > 2\sigma(I)$] reflections	36,119, 6550, 3674
T_{min}, T_{max}	0.685, 0.745
$(\sin\theta/\lambda)_{max}$ ($Å^{-1}$)	0.675
θ_{min}, θ_{max} (°)	1.8, 28.7
R_{int}	0.095
Refinement	
No. of parameters	352
$R[F^2 > 2\sigma(F^2)]$, $wR(F^2)$, S	0.081, 0.217, 1.04
$\Delta\rho_{max}$, $\Delta\rho_{min}$ (e $Å^{-3}$)	0.71, − 0.82
No. of reflections	6550
H-atom treatment	H-atom parameters constrained
CCDC Number	2,203,684

Statistical analyze

Data on antioxidants and metabolic enzymes were analyzed using one-way analysis of variance (ANOVA). The significance of the mean difference was assessed using Tukey's HSD test. In SPSS 15.0, all analyses were carried out (SPSS, Chicago, IL, USA). To determine whether the difference between the averages was significant, a probability level of 0.05 was used.

Results and discussion

X-ray structural determination

The experimental details are given in Table 1. There is only one half molecule in the asymmetric unit (Fig. 1). Title dinuclear Cu^{II} complex, (I), contains four 4-cyanobenzoate (CYNB) and four 4-cyanopyridine (CYNP) anions (Fig. 2). Each Cu(II) atom is coordinated through the oxygen atoms of the CYNB anion, and the monomers are bridged through the oxygens of the CYNB anions. The Cu^{II} atom is six coordinated, and Cu1·Cu1^{i} distance is 4.373(4) Å. The CYNB oxygens (O1, O2, O3 and O4^{i}) at distances of Cu1–O1 = 1.977 (3) Å, Cu1–O2 = 2.645 (3) Å, Cu1–O3 = 1.950 (3) Å and Cu1–O4 = 2.323 (4) Å in the equatorial plane around the Cu^{II} atom form a distorted square-planar arrangement, where the Cu^{II} atom is − 0.0132 (6) Å away from the best least-squares plane of the four oxygen atoms. The distorted octahedral coordination is completed by the two 4-cyanopyridine (CYNP) N atoms (N4 and N5) at distances of Cu1–N3 = 2.046 (4) Å and Cu1–N5 = 2.048 (4) Å in the axial positions with the average Cu–O and Cu–N bond lengths of 2.2238(3) Å and 2.047(4) Å, respectively (Table 2).

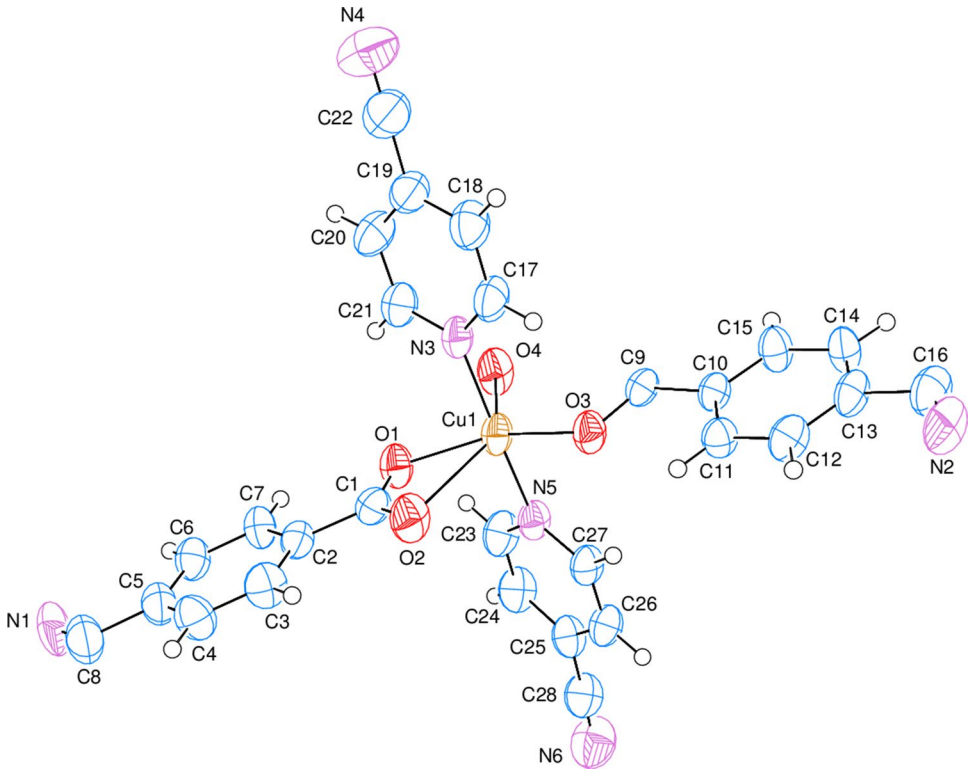

Fig. 1 The asymmetric unit of the title compound. Thermal ellipsoids are drawn at the 50% probability level

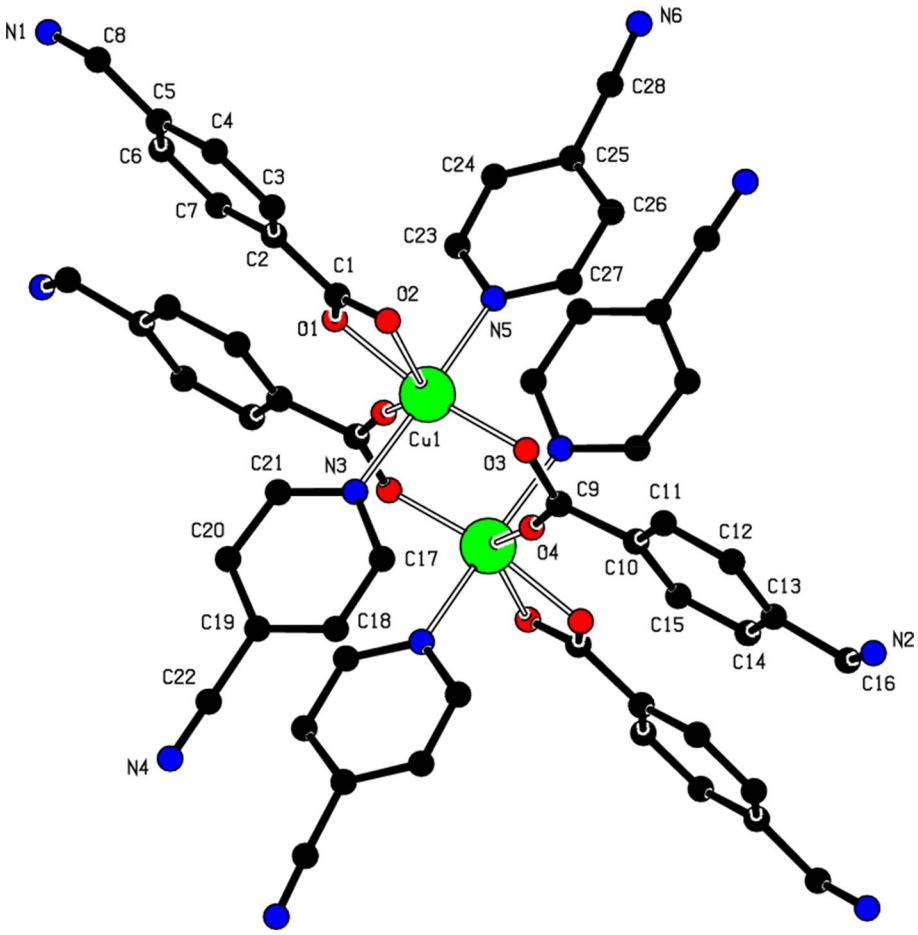

Fig. 2 The molecular diagram of the title compound [symmetry code: (i) − x + 2, − y, − z + 2]

Table 2 Selected geometric parameters (Å, °)

Cu1–O3	1.950 (3)	Cu1–O4	2.323 (4)
Cu1–O1	1.977 (3)	O1–C1	1.289 (6)
Cu1–N5	2.048 (4)	O2–C1	1.231 (6)
Cu1–N3	2.046 (4)		
O2···C27^{i}	3.058 (7)	N1···C2^{iv}	3.211 (7)
O2···C26^{i}	3.060 (6)	N1···C1^{iv}	3.244 (7)
O1···H23	2.58	N2···C24^{v}	3.156 (9)
O1···H21	2.50	N2···C23^{v}	3.213 (9)
O1···H7	2.47	N1···H6	2.60
H15···O1^{ii}	2.71	N1···H18^{iii}	2.42
O2···H3	2.52	N2···H23^{v}	2.77
O2···H27^{i}	2.44	N2···H24^{v}	2.67
O2···H26^{i}	2.48	N2···H12	2.65
O3···H17	2.47	H4···N4^{vi}	2.72
O3···H11	2.47	H20···N6^{vii}	2.67
O3···H27	2.46	C5···C16^{i}	3.465 (8)
O4···H21	2.80	C6···C19^{iv}	3.427 (8)
O4···H23	2.60	C9···C17	3.282 (6)
H15···O4^{ii}	2.49	C9···H17	2.71
N1···C18^{iii}	3.204 (7)		
O3–Cu1–O1	155.42 (16)	O3–Cu1–O4	117.47 (15)
O3–Cu1–N5	90.59 (15)	O1–Cu1–O4	86.96 (14)
O1–Cu1–N5	88.09 (16)	N5–Cu1–O4	86.53 (16)
O3–Cu1–N3	93.33 (16)	N3–Cu1–O4	85.44 (17)
O1–Cu1–N3	91.11 (16)	O2–C1–O1	123.4 (5)
N5–Cu1–N3	171.97 (17)		

Symmetry codes: (i) −x+1, −y, −z+2; (ii) −x+2, −y, −z+2; (iii) x−1, y, z−1; (iv) x−1/2, −y+1/2, z−1/2; (v) x, y, z+1; (vi) x−3/2, −y+1/2, z−1/2; (vii) −x+3/2, y+1/2, −z+3/2

Table 3 Hydrogen bond geometry (Å, °)

D–H···*A*	*D*–H	H···*A*	*D*···*A*	*D*–H···*A*
C18–H18···N1^{viii}	0.93	2.42	3.204 (7)	142
C11–H11···Cg4^{i}	0.93	2.78	3.670 (6)	159

Symmetry codes: (i) −x+1, −y, −z+2; (viii) x+1, y, z+1. Cg4 is the centroid of ring *D* (N5/C23–C27)

Cu^{II} is located out of the least-squares planes of (O1/C1/O2) and (O3/C9/O4) by 0.0653 (6) Å and -0.1671 (5) Å, respectively. The O1–Cu1–O2 angle is 55.15 (4)°. The corresponding O–M–O (where M is a metal) angles are 53.50 (14)°in $[Cu_2(FB)_4(INA)_4]$ (Sertçelik et al. 2013), 50.4 (2)° in $[Pb((BPDC)_4]_n$ (Sertçelik et al. 2012a), 87.54 (5)° in $[Cd(CB)_2(DENA)_2(H_2O)_2]$ (Akduran et al. 2016), 87.96 (3)° in $[Co(FB)_2(NA)_2(H_2O)_2]$ (Sertçelik et al. 2012c), 87.28 (3)° in $[Ni(FB)_2(NA)_2].H_2O$ (Sertçelik et al. 2012d), 91.84 (12)° in $[Co(FB)_2(DENA)_2]0.2H_2O$ (Sertçelik et al. 2009) [NA, INA, DENA, FB, BPDC and CB are nicotinamide, isonicotinamide, *N,N*-diethylnicotinamide, 4-formylbenzoate, 2–2′-bipyridine-5–5′-dicarboxylic, and 4-cyanobenzoate, respectively] and 55.2 (1)° in $[Cu(Asp)_2(py)_2]$ (where Asp is acetylsalicylate and py is pyridine) (Greenaway et al. 1984).

The similarities of the O1–C1 [1.289 (6) Å], O2–C1 [1.231 (6) Å] and O3–C9 [1.280 (6) Å], O4–C9^{i} [1.210 (6) Å] bonds indicate delocalized bonding arrangements, rather than localized single and double bonds. The O1–C1–O2 [123.4 (5)°] and O3–C9–O4^{i} [125.4 (4)°] bond angles are increased according to that in a free acid [122.2°], and also they may be compared with the corresponding value of 124.27 (17)° in diaquabis(2-bromo-benzoato-κO) bis(nicotinamide-κN^{1})zinc(II) (Hökelek et al. 2009a).

The (O1/C1/O2), (O3/C9/O4) groups and the adjacent benzene rings *A* (C2–C7) and *B* (C10–C15) are oriented by 1.21 (38)° and 4.37 (18)°, respectively, while the rings *A*, *B*, *C* (N3/C17–C21) and *D* (N5/C23–C27) are oriented by *A*/*B* = 7.95 (15)°, *A*/*C* = 79.38 (15)°, *A*/*D* = 87.09(14)°, *B*/*C* = 74.34 (15)°, *B*/*D* = 83.11(14)° and *C*/*D* = 12.40(20)°.

The carboxylate group and the benzene ring *C* (C9–C14) are oriented by 4.54 (8)°, while the rings *A* (C2–C7), *B* (O2/C1/C2/C7/C8) and *C* are oriented by *A*/*B* = 1.81(6)°, *A*/*C* = 46.26(6)° and *B*/*C* = 47.92(6)°. So, A and B rings are almost coplanar, and the almost coplanar group is oriented with respect to benzene, *C*, ring at a dihedral angle of 47.05 (5)°.

The molecules are connected in a network design, enclosing $R_2^2(34)$ ring motifs, in the crystal by weak C–H N hydrogen bonds (Table 3), which may help to stabilize the structure (Fig. 3). The crystal packing is further strengthened by a marginal C–H··· π interaction (Table 3).

Infrared spectra

The results of the complex's FT-IR spectrum are displayed in the Supplementary Figure. The carboxylate ion's coordination type is revealed by FT-IR spectroscopy. It is known to be possible to estimate the coordination types of the carboxylate group using the value, which is the difference between the asymmetric and symmetric stretching frequencies [as(COO) and s(COO)]. Carboxylate ligands' symmetric and asymmetric COO^- stretching vibrations were seen in bands at 1591 cm^{-1} and 1395 cm^{-1}, respectively. The difference between the asymmetric and symmetrical carboxylate vibrations was used to calculate the complex's value of v, and the resultant value of 196 cm^{-1} confirms the structure's bridging bidentate coordination of the carboxylate anions (Nakamoto 2006). The 3-cyanopyridine coordinates in the complex's structure, as evidenced by the strong cyano v(CN) peak visible at 2239 cm^{-1} (Silverstein and Webster 1997; Pavia et al. 2001; Nakamoto 2006; Sertçelik et al. 2020). The

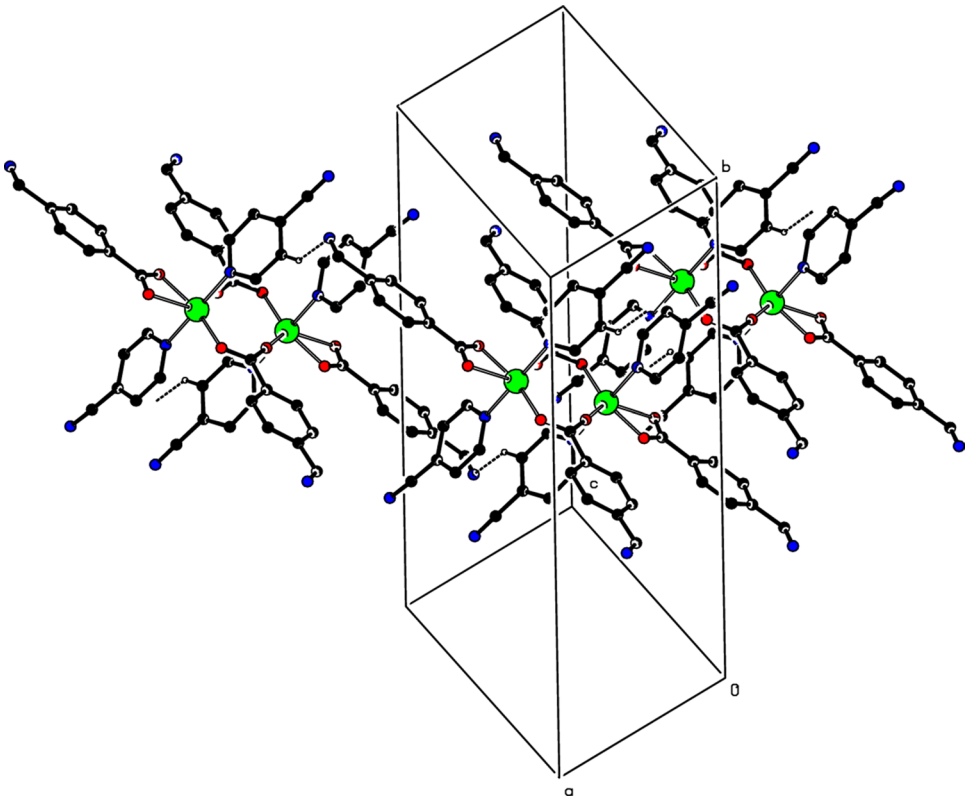

Fig. 3 A partial packing diagram. The C–H···N hydrogen bonds are shown as dashed lines. Nonbonding hydrogen atoms have been omitted for clarity

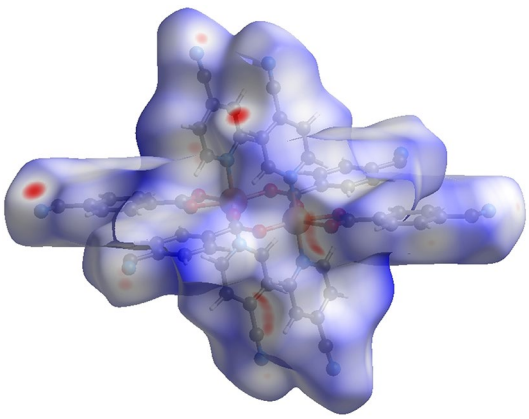

Fig. 4 View of the three-dimensional Hirshfeld surface of the title compound plotted over d_{norm} in the range of −0.2539 to 1.8350 a.u

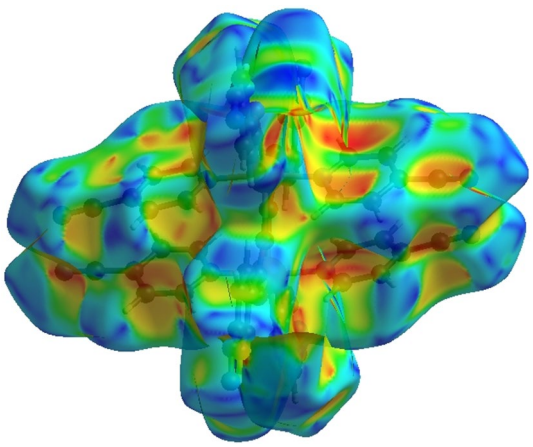

Fig. 5 Hirshfeld surface of the title compound plotted over shape index

peak at 691 cm^{-1} is shown by the Me-O bond's existence (Pavia et al. 2001).

Hirshfeld surface analysis

A Hirshfeld surface (HS) analysis (Hirshfeld 1977; Spackman and Jayatilaka 2009) was performed using Crystal Explorer 17.5 (Turner et al. 2017) to visualize the intermolecular interactions. In the HS plotted over d_{norm} (Fig. 4), the red and blue colors denote contacts with distances shorter (in close contact) or longer (in distinct contact), respectively, than the van der Waals radii, while the white surfaces denote contacts with distances equal to the sum of van der Waals radii (Venkatesan et al. 2016). The presence of adjacent red and blue triangles allows the shape index of the HS to be used as a tool to depict π π stacking; if there are no nearby red and/or blue triangles, then there are no π π interactions. There are no π π interactions, as Fig. 5

unequivocally demonstrates (I). On the other hand, the red triangle appeared on the right upper ring, *D* (N5/C23–C27), is the evidence of the C–H. π interaction (Table 3, Fig. 5) (Sreenatha et al. 2022; HariPrasad et al. 2023). The two-dimensional fingerprint plots provide the visual contents of the frequencies of the d_e and d_i combinations across the surface of the molecule, summarizing the complex information contained in the crystal. The color of each point corresponding to the relative area of each d_e and d_i combination is recognized as the contribution from different interatomic contacts, where blue, green and red corresponds to small, moderate and greatest contributions while an uncolored region indicates no contribution to the HS. Figure 6a shows the overall two-dimensional fingerprint plot. Figure 6b, c, d, e, f, i shows the relative contributions to the Hirshfeld surface of the contacts delineated into H···N/N···H, H···H, H···C/C···H, C···C, C···N/N···C, H···O/O···H, C···O/O···C and N···N contacts (McKinnon et al. 2007). With a contribution

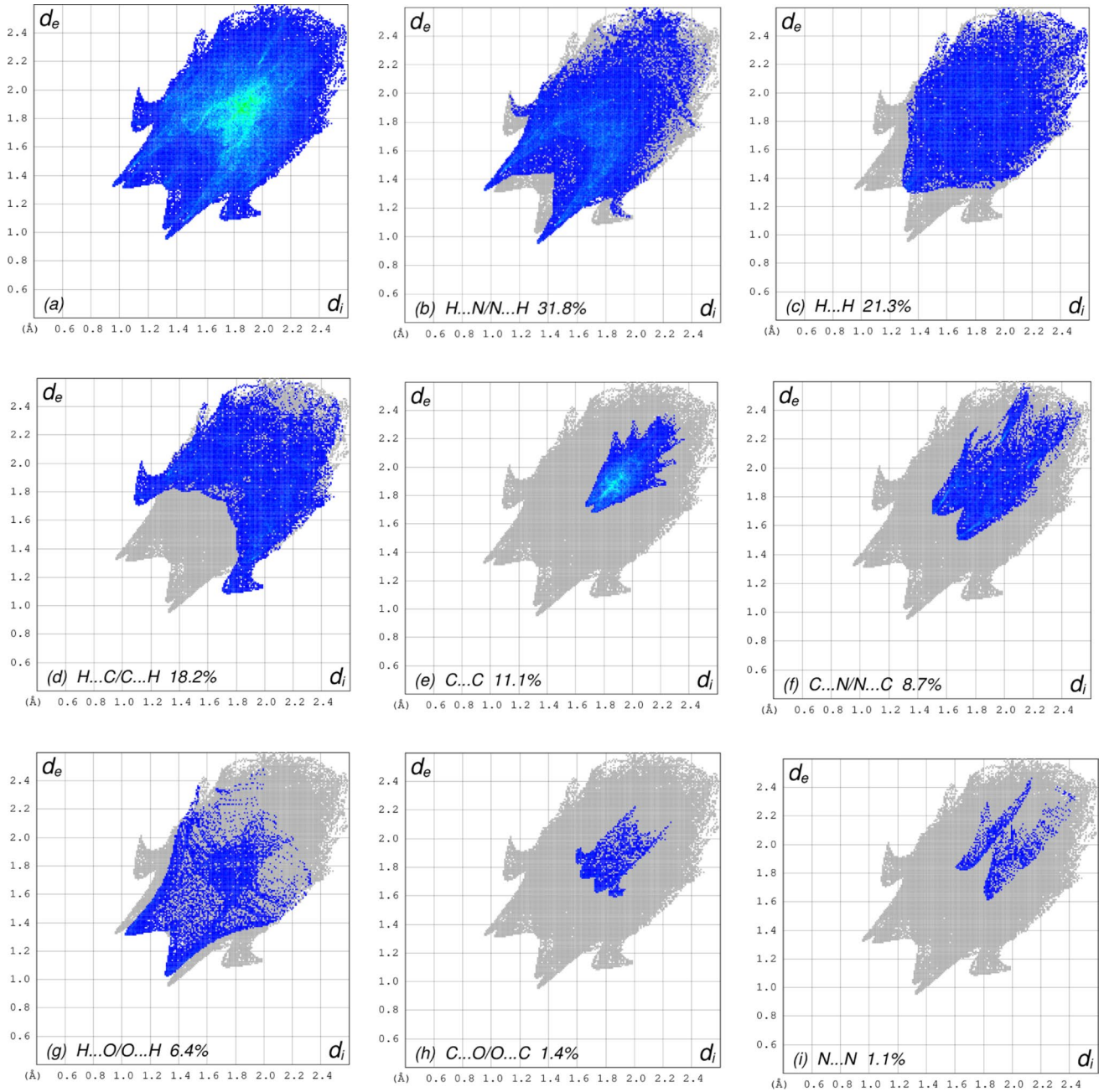

Fig. 6 The full two-dimensional fingerprint plots for the title compound, showing **a** all interactions, and delineated into **b** H···N/N···H, **c** H···H, **d** H···C/C···H, **e** C···C, **f** C···N/N···C, **g** H···O/O···H, **h** C···O/O···C and **i** N···N interactions. The d_i and d_e values are the closest internal and external distances (in Å) from given points on the Hirshfeld surface contacts

of 31.8%, the most significant interaction is H···N/N···H, which is depicted in Fig. 6b (Table 2) and can be visualized as a pair of spikes with the tips at $d_e + d_i = 2.27$ Å. The H ··· H interactions, with 21.3% contribution, are shown in Fig. 6c with the tip at $d_e = d_i = 1.32$ Å. The wings of H … C/C···H contacts with 18.2% contribution (Fig. 6d, Table 2) have the tips at $d_e + d_i = 2.80$ Å. The C···C contacts with 11.1% contribution (Fig. 6e, Table 2) are emerged with an arrow-shaped distribution of points at $d_e = d_i = 1.70$ Å. The 8.7% contribution of C···N/N···C contacts (Fig. 6f, Table 2) have tips at $d_e + d_i = 3.20$ Å. The H···O/O···H contacts (Fig. 6g), which account for 6.4% of the total, result from the H···O/O···H contacts (Table 2) and are shown as a pair of spikes with the tips located at $d_e + d_i = 2.32$ Å. Finally, the contributions of the C···O/O···C (1.4%, Table 2 and Fig. 6h) and N···N (1.1%, Fig. 6i) contacts to the HSs have scattered points of very low densities, less than 1.5%, with the tips located at $d_e + d_i = 3.35$ Å and 3.45 Å, respectively. The nearest neighbor coordination environment of a molecule is identified from the color patches on the Hirshfeld surface depending on their closeness to adjacent molecules. In Fig. 7 a, b, c and d, the Hirshfeld surface representations for the H···N/N···H, H···H, H···C/C···H and C···C interactions, respectively, are displayed with the function d_{norm} projected onto the surface.

The significance of H-atom contacts in creating the packing is supported by the Hirshfeld surface analysis. The abundance of H···N/N···H, H···H, and H···C/C···H interactions leads one to believe that hydrogen bonding and van der Waals interactions play a major role in the crystal packing (Hathwar et al. 2015).

Effects of complex on levels of metabolic enzymes and non-enzymatic antioxidant in hemolymph of G. mellonella

In the present study, transferase enzymes such as AST ($F_{3,12}$: 435.143, $p < 0.05$), ALT ($F_{3,12}$: 1822.27, $p < 0.05$) and GGT ($F_{3,12}$: 295.747, $p < 0.05$) levels increased significantly at the complex concentration of 3%, according to the control group (Figs. 8 A-C). Cell damage indicator LDH activity statistically increased in hemolymph of *G. mellonella* at 3% complex concentrations ($F_{3,12}$: 17.775, $p < 0.05$) (Fig. 8D). CK activity increased approximately twofold at the complex concentration of 3%, according to the control group ($F_{3,12}$: 356.779, $p < 0.05$) (Fig. 8E). ALP activity significantly increased at 0.3% and 3% complex concentrations ($F_{3,12}$: 73.086, $p < 0.05$) (Fig. 8F). The other metabolic enzyme

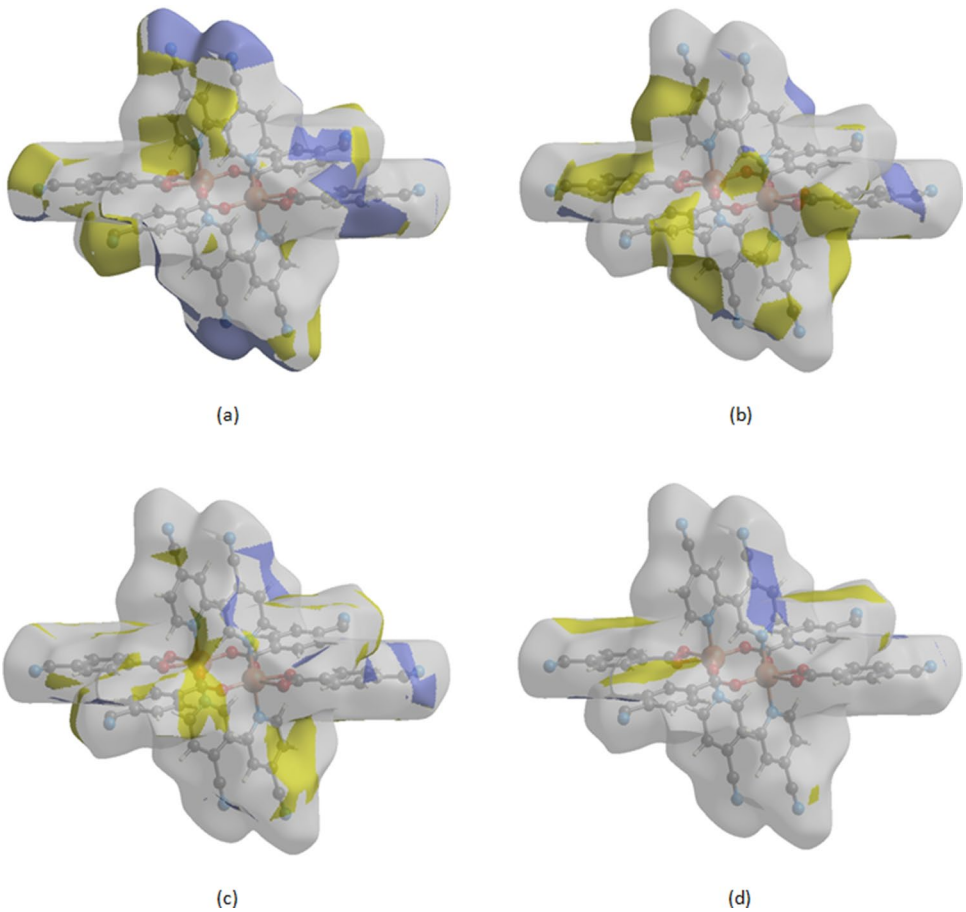

Fig. 7 The Hirshfeld surface representations with the function d_{norm} plotted onto the surface for **a** H···N/N···H, **b** H···H, **c** H···C/C···H and **d** C···C interactions

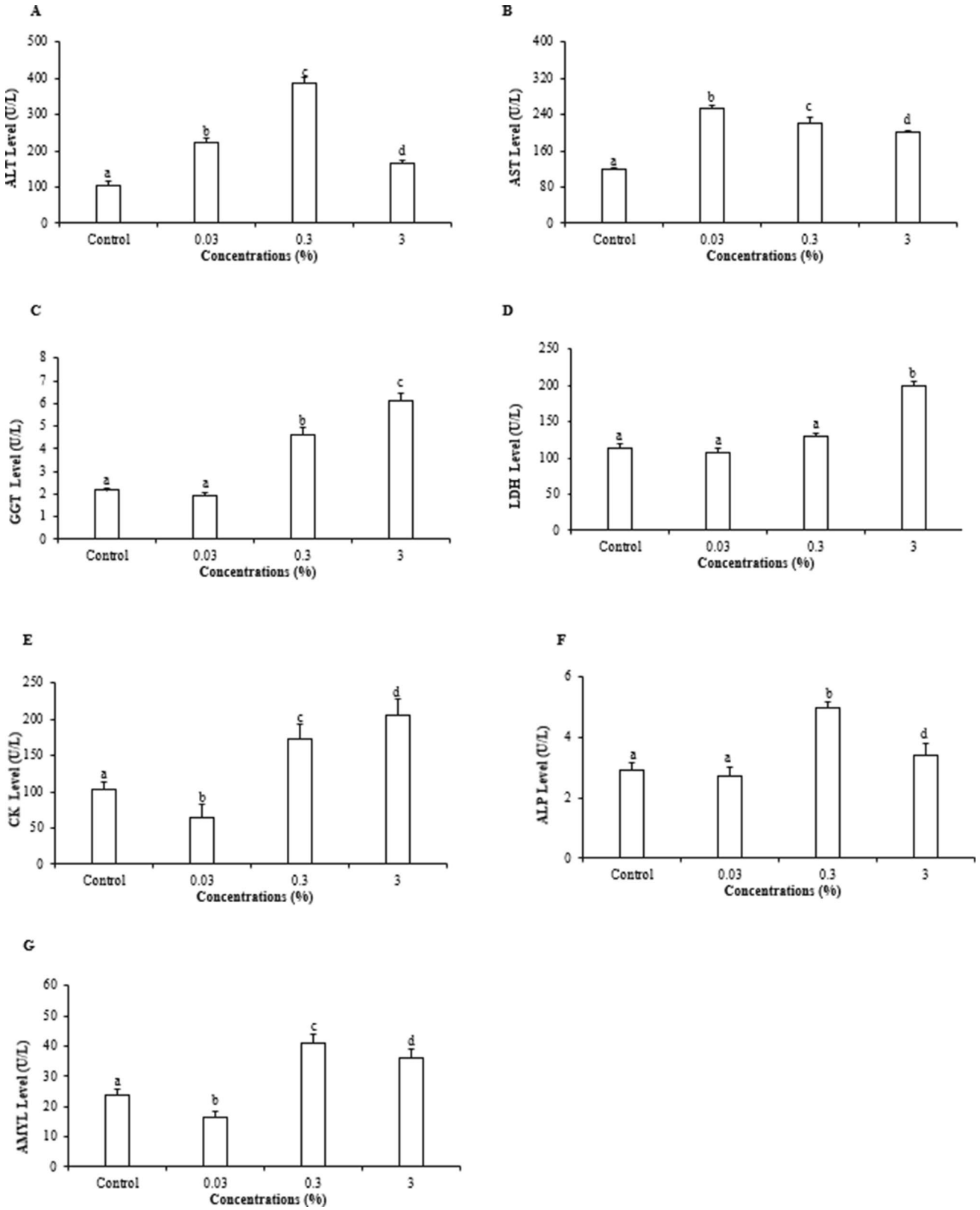

Fig. 8 Effects of Cu(II) 4-cyanobenzoate with 4-cyanopyridine complex on metabolic enzyme levels in hemolymph of *G. mellonella*. Bars represent the means (± S.E.) of four replicates. Means followed by the same letter are not significantly different ($P > 0.05$, Tukey's HSD test)

AMYL activity decreased at 0.03% complex concentration, but significantly increased at 0.3% and 3% complex concentrations ($F_{3,12}$: 118.752, $p < 0.05$) (Fig. 8G).

In the current study, non-enzymatic antioxidants were significantly increased in all complex treatments. The amount of ALB increased approximately fourfold at the complex concentration of 3%, according to the control group ($F_{3,12}$: 365.843, $p < 0.05$) (Fig. 9A). The amounts of UA ($F_{3,12}$: 96.721, $p < 0.05$) and BIL ($F_{3,12}$: 277.100, $p < 0.05$) significantly increased in hemolymph of *G. mellonella* at 3% complex concentration when compared to the control group (Fig. 9B and C).

Conclusions

One carboxylate group from a 4-cyanobenzoate anion chelates the Cu^{II} atom, which is coordinated by two 4-cyanopyridine anions; two carboxylate O atoms from the two 4-cyanobenzoate anions bridge to the Cu^{II} atom, completing the six-coordination geometry. The four carboxylate O atoms in the equatorial plane result in a distorted square-planar arrangement around the Cu^{II} atom, while the two 4-cyanopyridine N atoms in the axial locations complete the deformed octahedral coordination.

In this study, AST, ALT and LDH, cell damage indicators, levels significantly increased in the hemolymph of *G. mellonella* larvae. The reason for this increase may be cell damage due to the complex. In addition, the increase in ALP, CK and AMYL enzyme activities indicates that energy metabolism is impaired due to the oxidative damage. In another study, it was reported that the AST, ALT and LDH levels increased in the hemolymph of *G. mellonella* larvae due to the oxidative effect of the anthelmintic drug oxfendazole (Sugeçti and Büyükgüzel 2018). In another study, it was reported that the cell damage indicator LDH activity increased in *G. mellonella* larvae due to *Klebsiella pneumoniae* infection (Wand et al. 2013). In one of our early study, it was also reported that metabolic enzyme levels such as AST, ALT, LDH, CK and GGT increased in the hemolymph of *G. mellonella* larvae due to the oxidative effect of diaquabis-bis-cobalt complex (Sertçelik et al. 2018).

Enzymatic and non-enzymatic antioxidants play a key role in preventing oxidative damage. In the present study, the non-enzymatic antioxidant levels such as ALB, UA and BIL significantly increased in hemolymph of *G. mellonella*. This increase in non-enzymatic antioxidants may be for the

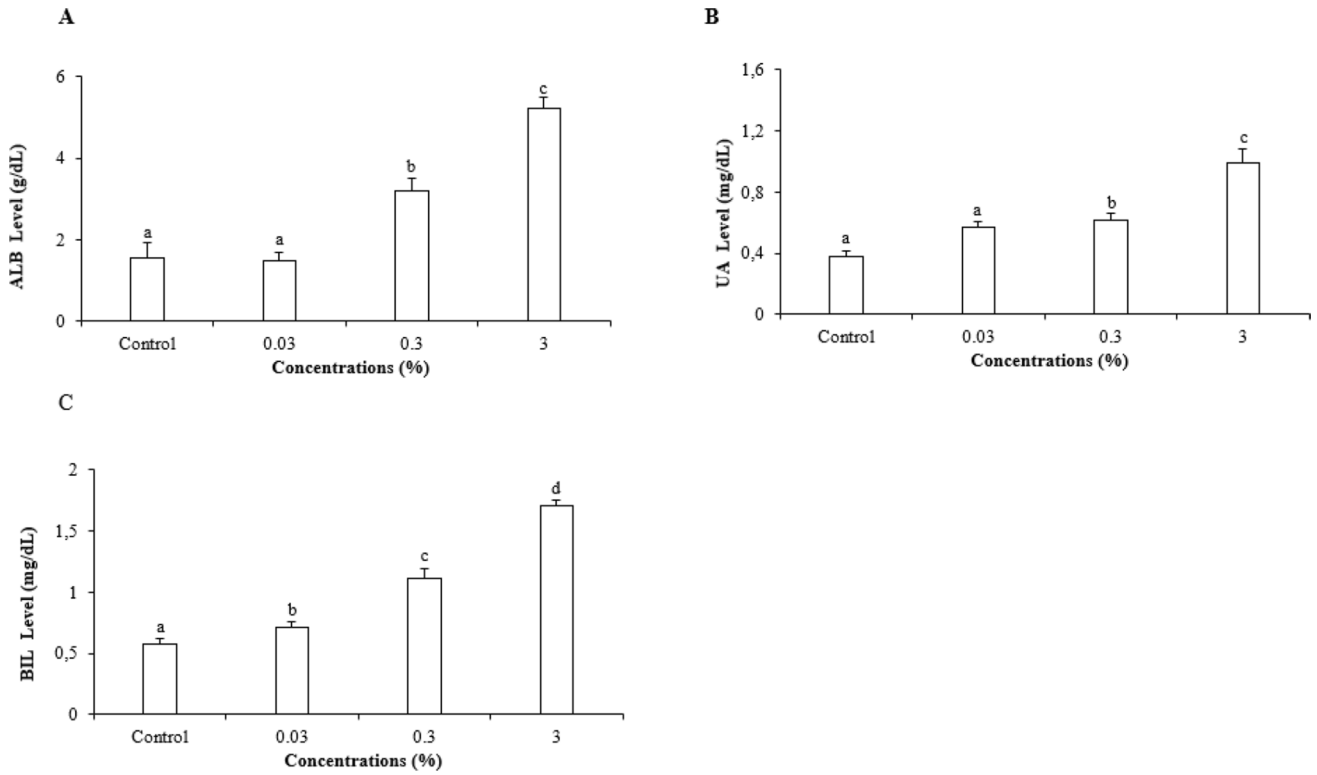

Fig. 9 Effects of Cu(II) 4-cyanobenzoate with 4-cyanopyridine complex on amount of non-enzymatic antioxidants in hemolymph of *G. mellonella*. Bars represent the means (±S.E.) of four replicates. Means followed by the same letter are not significantly different ($P > 0.05$, Tukey's HSD test)

prevention of oxidative damage. In another study, it was reported that the amount of UA and BIL increased in the hemolymph of *G. mellonella* larvae exposed to copper oxide nanoparticles (Tunçsoy et al. 2021). Sugeçti and coworkers were also reported that the amount of non-enzymatic antioxidants UA and BIL increased in *G. mellonella* larvae to protect against the oxidative effect of titanium nanoparticles. In another study, it was reported that the amount of antioxidants UA, ALB and BIL increased due to *Escherichia coli* infection (Sugeçti 2021a).

The findings demonstrated that complex causes cell damage, disrupts energy metabolism and alters the amounts of non-enzymatic antioxidants. We suggest that it can be an alternative chemical to insecticides against pests with good adjustment of complex concentrations.

Supplementary Information The online version contains supplementary material available at https://doi.org/10.1007/s11696-023-02865-6.

Acknowledgements Tuncer Hökelek is grateful to Hacettepe University Scientific Research Unit (Grant No. 013 D04 602 004).

Data availability The data that supports the findings of this study are available in the supplementary material of this article.

Declarations

Conflict of interest The authors declare that they have no known competing financial interests or personal relationships that could have appeared to influence the work reported in this paper.

References

Akduran N, Sertçelik M, Aydoğdu Ö, Necefoğlu H, Hökelek T (2016) Crystal structure of trans-diaquabis(4-cyanobenzoato-κO)bis(N,N-diethylnicotinamide-κN)cadmium. Acta Cryst E 72:1827–1829. https://doi.org/10.1107/S2056989016018247

Altuntaş H, Gwokyalya R, Bayram N (2022) Immunotoxic effects of force-fed ethephon on model organism *Galleria mellonella* (Lepidoptera: Pyralidae). Drug Chem Toxicol 45:1761–1768. https://doi.org/10.1080/01480545.2021.1873358

Bronskill, (1961) A cage to simplify the rearing of the greater wax moth, *Galleria mellonella* (Pyralidae). J Lep Soc 15(2):102–104

Bruker (2012) APEX2, SAINT and SADABS V2014/4.

Büyükgüzel E, Büyükgüzel K (2021) Oxidative impact of dietary triclabendazole in galleria mellonella. Kafkas Univ Vet Fak Derg. https://doi.org/10.9775/kvfd.2020.25170

Danouche M, El Ghachtouli N, El Baouchi A, El Arroussi H (2020) Heavy metals phycoremediation using tolerant green microalgae: Enzymatic and non-enzymatic antioxidant systems for the management of oxidative stress. J Environ Chem Eng 8:104460. https://doi.org/10.1016/j.jece.2020.104460

El-Shwiniy WH, Elwahed MGA, Saeed RM, Zordok WA, El-Desoky SI (2021) Structural elucidation, molecular modeling, and biological and antioxidant studies of phenanthroline/nicotinamide metals complexes. Appl Organomet Chem 35:e6231. https://doi.org/10.1002/aoc.6231

Farrugia LJ (2012) WinGX and ORTEP for Windows: an update. J Appl Cryst 45:849–854. https://doi.org/10.1107/S0021889812029111

Gebremariam A, Chekol Y, Assefa F (2021) Isolation, characterization, and bio-insecticidal efficiency of Ethiopian isolates of Bacillus thuringiensis against *Galleria mellonella* L. (Lepidoptera: Pyralidae) and tomato whitefly, Bemisia tabaci (Genn.) (Hemiptera: Aleyrodidae). Egypt J Biol Pest Control 31:28. https://doi.org/10.1186/s41938-021-00375-9

Greenaway FT, Pezeshk A, Cordes AW, Noble MC, Sorenson JRJ (1984) Characterization of a mononuclear copper carboxylate complex: Bis(acetylsalicylato)bis(pyridine)copper(II). Inorg Chim Acta 93:67–71. https://doi.org/10.1016/S0020-1693(00)87890-1

Haida Z, Hakiman M (2019) A comprehensive review on the determination of enzymatic assay and nonenzymatic antioxidant activities. Food Sci Nutr 7:1555–1563. https://doi.org/10.1002/fsn3.1012

HariPrasad S, Sreenatha NR, Suchithra B, Nagesh Babu R, Suman GR, Lakshminarayana BN, Jeevan Chakravarthy AS (2023) Synthesis, structural and computational studies of a novel anionic synthon and its derivatives. J Mol Struct 1275:134558. https://doi.org/10.1016/j.molstruc.2022.134558

Hathwar VR, Sist M, Jørgensen MRV, Mamakhel AH, Wang X, Hoffmann CM, Sugimoto K, Overgaard J, Iversen BB (2015) Quantitative analysis of intermolecular interactions in orthorhombic rubrene. IUCrJ 2:563–574. https://doi.org/10.1107/S2052252515012130

Hirshfeld FL (1977) Bonded-atom fragments for describing molecular charge densities. Theoret Chim Acta 44:129–138. https://doi.org/10.1007/BF00549096

Hökelek T, Dal H, Tercan B, Özbek FE, Necefoğlu H (2009a) Diaquabis(2-bromo benzoato-κO)bis(nicotinamide-κN^1)zinc(II). Acta Crystallogr Sect E-Crystallogr Commun 65:m607–m608. https://doi.org/10.1107/S1600536809015645

Hökelek T, Yilmaz F, Tercan B, Ozbek FE, Necefoglu H (2009b) Diaquabis(2-bromobenzoato-κO)bis(nicotinamide-κN^1)nickel(II). Acta Crystallogr Sect E-Crystallogr Commun 65:m768–m769. https://doi.org/10.1107/S1600536809021710

Hökelek T, Yılmaz F, Tercan B, Sertçelik M, Necefoğlu H (2009c) catena-Poly[[(4-formylbenzoato-κO^1)(isonicotinamide-κN^1)zinc(II)]-μ-4-formylbenzoato-κ$^2O^1$:$O^{1'}$]. Acta Cryst E 65:m1399–m1400. https://doi.org/10.1107/S160053680904241X

Kastamonuluoğlu S, Büyükgüzel K, Büyükgüzel E (2020) The use of dietary antifungal agent terbinafine in artificial diet and its effects on some biological and biochemical parameters of the model organism *Galleria mellonella* (Lepidoptera: Pyralidae). J Econ Entomol 113:1110–1117. https://doi.org/10.1093/jee/toaa039

Li G, Zhu Z-Q, Chen Q, Li J (2019) Metal complex based delayed fluorescence materials. Org Electron 69:135–152. https://doi.org/10.1016/j.orgel.2019.02.022

McKinnon JJ, Jayatilaka D, Spackman MA (2007) Towards quantitative analysis of intermolecular interactions with Hirshfeld surfaces. Chem Commun (camb) 37:3814–3816

Nakamoto K (2006) Infrared and Raman Spectra of Inorganic and Coordination Compounds. In: Handbook of Vibrational Spectroscopy. American Cancer Society

Narayana SL, Sung-Ok B (2017) Anti-bacterial, anti-fungal and cytotoxic activities of hydrazones and their metal complexes: a review. Res J Biotechnol 12:66–76

Öztürkkan Özbek FE, Sertçelik M, Yüksek M, Elmalı A, Şahin E (2020) The superiority of the classical synthesis compared to the hydrothermal synthesis upon the structural, optical absorption and fluorescent properties of new Cd(II) 3-fluorobenzoate complexes with Pyridine-3-carboxamide/Pyridine-3-carboxylate. Inorg Chim Acta 509:119694. https://doi.org/10.1016/j.ica.2020.119694

Pavia DL, Lampman GM, Kriz GS (2001) Introduction to spectroscopy a guide for students of organic chemistry, 3rd ed. Fort Worth Harcourt College Publishers

Sertçelik M (2021) Synthesis, spectroscopic properties, crystal structures, DFT studies, and the antibacterial and enzyme inhibitory properties of a complex of Co(II) 3,5-difluorobenzoate with 3-pyridinol. J Chem Res 45:42–48. https://doi.org/10.1177/1747519820924636

Sertçelik M, Durman M (2020) Synthesis, characterization, and antibacterial activity of Cd(II) complexes with 3-/4-fluorobenzoates and 3-hydroxypiridine as co-ligands. Russ J Inorg Chem 65:1351–1359. https://doi.org/10.1134/S0036023620090168

Sertçelik M, Tercan B, Şahin E, Necefoğlu H, Hökelek T (2009) Diaquabis(N, N-diethylnicotinamide-κ^N1)bis(4-formylbenzoato-κO)cobalt(II). Acta Cryst E 65:m389–m390. https://doi.org/10.1107/S1600536809008265

Sertçelik M, Çaylak Delibaş N, Çevik S, Necefoğlu H, Hökelek T (2012a) Poly[(μ5-2,2′-bipyridine-5,5′-dicarboxylato)lead(II)]. Acta Cryst E 68:m1196–m1197. https://doi.org/10.1107/S1600536812035647

Sertçelik M, Çaylak Delibaş N, Necefoğlu H, Hökelek T (2012b) Diaquabis(4-formylbenzoato-κO^1)bis(nicotinamide-κN^1) nickel(II). Acta Cryst E 68:m946–m947. https://doi.org/10.1107/S1600536812026943

Sertçelik M, Çaylak Delibaş N, Necefoğlu H, Hökelek T (2012c) Diaquabis(4-formylbenzoato-κO^1)bis(nicotinamide-κN^1) cobalt(II). Acta Cryst E 68:m1091–m1092. https://doi.org/10.1107/S1600536812032205

Sertçelik M, Çaylak Delibaş N, Necefoğlu H, Hökelek T (2013) Bis(μ-4-formylbenzoato-κ^2O:O′)bis[(4-formylbenzoato-κ^2O, O′)bis(isonicotinamide-κN1)copper(II)]. Acta Cryst E 69:m290–m291. https://doi.org/10.1107/S1600536813010908

Sertçelik M, Özbek FE, Yüksek M, Elmalı A, Aydoğdu Ö, Necefoğlu H, Hökelek T (2020) Synthesis, spectral, thermal, structural, optical characterization, and Hirshfield surface analysis of N, N'-diethylnicotinamide complexes of Mn(II) and Co(II) 4-cyanobenzoates. Chem Pap 74:2021–2033. https://doi.org/10.1007/s11696-019-01040-0

Sertçelik M, Öztürkkan Özbek FE, Taslimi P, Necefoglu H, Hökelek T (2021) Supramolecular complexes of Ni (II) and Co (II) 4-aminobenzoate with 3-cyanopyridine: synthesis, spectroscopic characterization, crystal structure, and enzyme inhibitory properties. Appl Organomet Chem 35:e6182. https://doi.org/10.1002/aoc.6182

Sertçelik M, Sugeçti S, Büyükgüzel E, Necefoğlu H, Büyükgüzel K, (2018) Diaquabis N, N-dietilnikotinamid-lN1 bis 4-formilbenzoato-lO kobalt II Kompleksinin Model Organizma Galleria mellonella L. Lepidoptera: Pyralidae Üzerindeki Toksikolojik ve Fizyolojik Etkileri. Karaelmas Fen Ve Mühendislik Dergisi 8:359–364

Sheldrick GM (2015a) SHELXT-Integrated space-group and crystal-structure determination. Acta Cryst A71:3–8. https://doi.org/10.1107/S2053273314026370

Sheldrick GM (2015b) Crystal structure refinement with SHELXL. Acta Cryst C71:3–8. https://doi.org/10.1107/S2053229614024218

Silverstein RM, Webster FX (1997) Spectroscopic Identification of Organic Compunds. Canada

Spackman MA, Jayatilaka D (2009) Hirshfeld surface analysis. CrystEngComm 11:19–32. https://doi.org/10.1039/B818330A

Spek AL (2009) Structure validation in chemical crystallography. Acta Cryst D 65:148–155. https://doi.org/10.1107/S090744490804362X

Sreenatha NR, Ganesha DP, Jeevan Chakravarthy AS, Suchithra B, Lakshminarayana BN (2022) X-ray structure, Hirshfeld surfaces and interaction energy studies of 2,2-diphenyl-1-oxa-3-oxonia-2-boratanaphthalene. Heliyon. https://doi.org/10.1016/j.heliyon.2022.e10151

Sugeçti S (2021a) Biochemical and immune responses of model organism *Galleria mellonella* after infection with *Escherichia coli*. Entomol Exp Appl 169:911–917. https://doi.org/10.1111/eea.13092

Sugeçti S (2021b) Pathophysiological effects of Klebsiella pneumoniae infection on *Galleria mellonella* as an invertebrate model organism. Arch Microbiol 203:3509–3517. https://doi.org/10.1007/s00203-021-02346-y

Sugeçti S, Büyükgüzel K (2018) Effects of Oxfendazole on metabolic enzymes in hemolymph of *Galleria mellonella* L. (Lepidoptera: Pyralidae) larvae reared on artificial diet: oksfendazolün yapay besinde yetiştirilen *Galleria mellonella* L. (Lepidoptera: Pyralidae) larvalarinin hemolenf dokusundaki metabolik enzimler üzerine etkisi. Karaelmas Sci Eng J 8:590–594. https://doi.org/10.7212/zkufbd.v8i2.1380

Sugeçti S, Büyükgüzel K (2022) Effects of Ni (II) p-hydroxybenzoate with caffeine on metabolic, antioxidant, andbiochemical parameters of model insect *Galleria mellonella* L. (Lepidoptera: Pyralidae). Turkish Journal of Zoology 46:167–174. https://doi.org/10.3906/zoo-2110-6

Topal T (2022) Synthesis, X-ray, characterization and HSA and energy framework analysis of novel pyridine-hydrazone based ligand and its Co(II) complex biological activity prediction and experimental antibacterial properties. Mol Crystals and Liquid Crystals. https://doi.org/10.1080/15421406.2022.2060617

Tunçsoy B, Sugeçti S, Büyükgüzel E, Özalp P, Büyükgüzel K (2021) Effects of copper oxide nanoparticles on immune and metabolic parameters of *Galleria mellonella* L. Bull Environ Contam Toxicol 107:412–420. https://doi.org/10.1007/s00128-021-03261-0

Turner MJ, McKinnon JJ, Wolff SK, Grimwood DJ, Spackman PR, Jayatilaka D, Spackman MA (2017) CrystalExplorer17. University of Western Australia

Uddin MN, Ahmed SS, Alam SMR (2020) REVIEW: Biomedical applications of Schiff base metal complexes. J Coord Chem 73:3109–3149. https://doi.org/10.1080/00958972.2020.1854745

Venkatesan P, Thamotharan S, Ilangovan A, Liang H, Sundius T (2016) Crystal structure, Hirshfeld surfaces and DFT computation of NLO active (2E)-2-(ethoxycarbonyl)-3-[(1-methoxy-1-oxo-3-phenylpropan-2-yl) amino] prop-2-enoic acid. Spectrochim Acta Part A Mol Biomol Spectrosc 153:625–636

Wand ME, McCowen JWI, Nugent PG, Sutton JM (2013) Complex interactions of Klebsiella pneumoniae with the host immune system in a *Galleria mellonella* infection model. J Med Microbiol 62:1790–1798. https://doi.org/10.1099/jmm.0.063032-0

Zeng Z, Cai J, Li F, Weng Y, Huang Q, Yang H, Huang Q, Wei Y (2021) Synthesis, crystal structures, DNA interactions, and antitumor activity of two new dinuclear copper(II) complexes with thiazole ligand. RSC Adv 11:40040–40050. https://doi.org/10.1039/d1ra05798g